



Article

---

# Detection of Cavities from Dental Panoramic X-ray Images Using Nested U-Net Models

---

Shuaa S. Alharbi, Athbah A. AlRugaibah, Haifa F. Alhasson and Rehan Ullah Khan



<https://doi.org/10.3390/app132312771>

## Article

# Detection of Cavities from Dental Panoramic X-ray Images Using Nested U-Net Models

Shuaa S. Alharbi \* , Athbah A. AlRugaibah, Haifa F. Alhasson  and Rehan Ullah Khan 

Department of Information Technology, College of Computer, Qassim University, Buraydah 52571, Saudi Arabia; 421200031@qu.edu.sa (A.A.A.); hhson@qu.edu.sa (H.F.A.); re.khan@qu.edu.sa (R.U.K.)

\* Correspondence: shuaa.s.alharbi@qu.edu.sa

**Abstract:** Dental caries is one of the most prevalent and chronic diseases worldwide. Dental X-ray radiography is considered a standard tool and a valuable resource for radiologists to identify dental diseases and problems that are hard to recognize by visual inspection alone. However, the available dental panoramic image datasets are extremely limited and only include a small number of images. U-Net is one of the deep learning networks that are showing promising performance in medical image segmentation. In this work, different U-Net models are applied to dental panoramic X-ray images to detect caries lesions. The Detection, Numbering, and Segmentation Panoramic Images (DNS) dataset, which includes 1500 panoramic X-ray images obtained from Ivisionlab, is used in this experiment. The major objective of this work is to extend the DNS Panoramic Images dataset by detecting the cavities in the panoramic image and generating the binary ground truth of this image to use as the ground truth for the evaluation of models. These ground truths are revised by experts to ensure their robustness and correctness. Firstly, we expand the Panoramic Images (DNS) dataset by detecting the cavities in the panoramic images and generating the images' binary ground truth. Secondly, we apply U-Net, U-Net++ and U-Net3+ to the expanded DNS dataset to learn the hierarchical features and to enhance the cavity boundary. The results show that U-Net3+ outperforms the other versions of U-Net with 95% in testing accuracy.



**Citation:** Alharbi, S.S.; AlRugaibah, A.A.; Alhasson, H.F.; Khan, R.U. Detection of Cavities from Dental Panoramic X-ray Images Using Nested U-Net Models. *Appl. Sci.* **2023**, *13*, 12771. <https://doi.org/10.3390/app132312771>

Academic Editor: Nikolaos Kourkoumelis

Received: 16 October 2023

Revised: 18 November 2023

Accepted: 24 November 2023

Published: 28 November 2023



**Copyright:** © 2023 by the authors. Licensee MDPI, Basel, Switzerland. This article is an open access article distributed under the terms and conditions of the Creative Commons Attribution (CC BY) license (<https://creativecommons.org/licenses/by/4.0/>).

**Keywords:** artificial intelligence; dental caries; deep learning; dental panoramic X-ray images; image segmentation; machine learning; medical image; nested U-Net models; U-Net3+

## 1. Introduction

Tooth decay, also known as dental caries, is a widespread and long-lasting health issue across the globe [1,2]. According to the International Caries Detection and Assessment System (ICDAS) [3], dental caries can be described as a loss of minerals in the hard tissues of the teeth due to a combination of factors, including biofilm formation, dietary choices, and various other factors. These factors encompass biological, behavioral, psychological, and environmental aspects. The end result of this process is the development of a caries lesion, which can affect both primary and permanent teeth, leading to damage in the tooth's crown and exposure of the root surfaces [4]. These lesions begin with the demineralization of tooth surfaces, ultimately progressing into larger cavities and potentially causing pulpitis [5].

As such, timely detection can prevent tooth damage and save expensive healthcare costs. Thus, an effective method for early dental caries detection is a crucial subject in dental research. Over the past years, visual inspection, tactile examinations, radiograph methods, and the use of a dental probe were the most common methods for determining caries lesions with the help of radiography and dental explorers [5,6]. These traditional caries detection methods are effective for large, clearly visible caries and partially obscured caries that are detectable using a handheld mirror [6]. Inspection using radiographic imaging indicates the locations of suspicious lesions, and tactile examination helps dentists access

carious lesions directly. This methodology has some drawbacks, however. It is impossible to trace subtle lesions because X-ray images show a two-dimensional (2D) representation of three-dimensional (3D) tooth structures. Moreover, the tactile examination is experimental and depends on intuition, and not on quantifiable standards [5]. Radiographic detection requires ionizing radiation, which can deposit energy in human cells and cause tissue change [7]. In addition, for different practitioners, even when using the same radiograph, discrepancies in caries detection can be caused by factors such as the radiograph quality, viewing conditions, and the dentist's expectations and experience [8].

In recent years, artificial intelligence (AI) has become more popular and widely applied in different medicine fields, such as the liver [9], breast [10] and dentistry [11,12]. Among the wide scope of applications in dentistry, AI has shown good performance in detecting carious lesions [13]. The convolutional neural network (CNN)-based models have shown to detect caries lesions with superior performance. The augmentation and integration of AI in dental care is a relatively new paradigm and needs to be expedited and further explored [14]. CNNs have recently been integrated to solve a number of medical problems stages [15] due to the ability to handle complex tasks, and they have been shown to provide accurate detection with improved clinical outcomes [16–19]. U-Net is a popular convolutional neural network architecture known for its effectiveness in medical image segmentation tasks. It is a commonly used CNN architecture for medical image segmentation, known for its effectiveness in pixel-level classification and its flexibility in handling both 2D and 3D medical images [20]. Several medical image segmentation algorithms use the U-Net encoder-decoder architecture [21,22]. To capture fine-grained semantics and coarse-grained details, U-Net3+ [23] improves the U-Net.

In dentistry, the use of CNN has been investigated since 2015. Ronneberger et al. [21] proposed the U-Net to analyze dental structure segmentation on bitewing radiographs. There have, however, been limited studies evaluating U-Net or CNN-based U-Net architectures for the detection of dental caries. In addition, there are very few datasets available for dental panoramic X-ray images. Therefore, we focus in a similar direction to contribute to the state of the art by utilizing the U-Net shape-based approach for dental cavity detection. We believe that this work will help healthcare professionals and dental practitioners detect dental caries. Furthermore, it may serve for the appraisal and comparative analysis of emerging methodologies within this domain.

Efforts to develop techniques for the cavity detection task have been previously described in the literature [11]. Cavity detection methods have focused on classifying teeth as decayed or normal. One of the early trials of the use of neural networks (NNs) to classify cavities was by [24]. They proposed a NNs-based tooth decay diagnostic system in which they used normalized auto-correlation coefficients to distinguish decayed teeth and normal teeth. The back propagation algorithm was used to construct the weights for the NN classifier in this system. Additionally, Ali et al. [25] classified dental X-rays into normal or decayed teeth images. They proposed a system of detecting dental caries and classifying X-ray images using deep NNs. The deep NNs technique was based on a stacked sparse auto-encoder containing three hidden layers for features extraction and a Soft-Max classifier to classify the teeth images into decayed teeth or normal teeth. This approach showed good detection performance and obtained an accuracy score of 97%.

Later, Casalegno et al. [6] introduced the DL model based on a CNN for the detection and localization of dental lesions in Near-Infrared Light Transillumination (NILT) images. Their study assessed the model's performance in two key aspects: pixel-wise segmentation into tissue classes and binary labeling, and distinguishing between healthy and diseased regions of interest. The results demonstrated that employing a DL approach for analyzing dental images yielded favorable outcomes, providing valuable support for dental practitioners [6].

Similarly, Schwendicke et al. [26] applied deep CNNs to identify caries lesions in NILT images. They conducted training using two different CNN architectures, Resnet18 and Resnet50, and validated the model's performance through a 10-fold cross-validation process.

The findings indicated that both models performed comparably in predicting caries in tooth segments within NILT images. Notably, Resnet50 exhibited slightly superior performance, as measured by the area under the receiver operating characteristic curve (AUC) [26].

Haghanifar et al. [27] proposed a network for detecting caries in panoramic dental X-rays (PaXNet), which is composed of two main modules: the feature extraction module and the classification module. In the feature extraction block, three pretrained models were used: Encoder, CheXNet, and InceptionNet, where SoftMax is used as a classifier. Lian et al. [28] used DL for the detection of caries lesions and the classification of radiographic extensions on panoramic films. The dataset consisted of 1160 panoramic films. A CNN NNU-Net was used in the detection process, and DenseNet-121 was used for the classification step according to their depths. The accuracy and recall rate of NNU-Net were 0.986 and 0.821, respectively. Moran et al., in their study, [29] successfully identified approximal dental caries in bitewing images and sorted them based on the condition of the lesion. They conducted classification model evaluations employing Inception and ResNet architectures, considering three different learning rates: 0.1, 0.01, and 0.001. Kuhnisch et al. [30] used oral photographs to detect and classify cavities as caries-free, non-cavitated caries lesions, or caries-related cavitation. To train AI methods cyclically and repeatedly, each expert diagnosis was used as a reference standard.

Currently, deep learning (DL) methods have gained popularity among researchers due to their exceptional performance and increased accuracy when trained with substantial amounts of data. In the study by Lee et al. [31], the effectiveness of deep CNN algorithms to detect dental caries in periapical X-ray images was examined. They employed a pre-trained GoogLeNet Inception v3 CNN network for pre-processing and transfer learning. The dataset utilized in this investigation consisted of 3000 periapical images, with 2400 images in the training set and 600 in the testing set. The accuracy for detecting premolar caries was 89.0 percent, while for molar caries, it was 88.0 percent. The combined premolar and molar model achieved an accuracy of 82.0 percent. Notably, the premolar model exhibited the highest Area Under the Curve (AUC) at 0.917, demonstrating its strong performance in caries detection in periapical X-ray images. This study highlights the effectiveness of deep CNN algorithms in this application. Similarly, in another study conducted by Zhang et al. [32], a deep learning system based on a CNN was developed and evaluated for the detection of dental caries. The system was trained and tested on a dataset comprising 3932 photographs taken by 625 volunteers.

Other researchers aim to solve the problem of cavity detection by providing a prediction of the needed treatment. Bouchahma et al. [33] proposed an automatic method to detect dental decay in order to predict the necessary treatment. This method predicted three types of treatments: (1) fluoride, (2) filling, and (3) root canal treatments. The proposed method classified the X-ray images among the three treatments. The overall accuracy of the model reached 87 percent. The best prediction was for the fluoride treatment with an accuracy score of 98 percent, followed by the root canal detection with an accuracy score of 88 percent. The filling treatment gave a lower classification accuracy score of 77 percent. Some researchers viewed the cavity detection problem as being one of segmentation. U-Net is widely applied for segmentation tasks in medical imaging [21,34].

In the field of dental image analysis, several notable studies have utilized the U-Net architecture. Sivagami et al. [35] employed the U-Net with CNN to accurately segment dental panoramic X-ray images, achieving superior results compared to other segmentation methods. They used the Ivisionlab dataset, which includes both X-ray and ground truth images. Furthermore, Zheng et al. [14] proposed an innovative algorithm that integrates oral anatomical knowledge with deep learning to segment CBCT and detect lesion. They improved on traditional U-Net by incorporating Fully Convolutional DenseNet (Dense U-Net), demonstrating enhanced lesion detection accuracy. Furthermore, Cantu et al. [36] focused on detecting caries lesions on bitewing X-rays using the U-Net model, achieving a pixel-wise marking accuracy of 0.80 percent with the Intersection-over-Union metric. Later, Lee et al. [8] applied the U-Net model for the detection of dental caries using bitewing

radiographs. Their results showed a precision score of 63.29 percent, a recall score of 65.02 percent, and an F1 score of 64.14 percent. In particular, dentist diagnostic performance improved when using the CNN model's results as a reference for caries detection, especially in proximal regions that are challenging to identify due to various factors, such as uneven exposure to X-rays and natural variability in tooth density or thickness.

In addition, Khan et al. [37] investigated automated feature detection, segmentation, and quantification of common findings by using DL-based computer vision techniques. The approaches based on the U-Net architecture showed the best results in medical applications. The overall best-performing architecture in the validation dataset was U-Net with DenseNet121. Zhu et al. [38], to distinguish various caries degrees from panoramic radiographs, suggested a unique deep learning architecture dubbed CariesNet. First, they gathered a high-quality panoramic radiograph dataset with 3127 clearly defined caries lesions that encompass shallow, intermediate, and deep caries. The model was trained using 304 radiographs and achieved a precision of 63.29%, recall of 65.02%, and F1-score of 64.14% on the test dataset. In addition, the diagnostic performance of all three clinicians improved significantly when they referred to the results of the CNN model. This improvement was particularly noticeable in their ability to detect initial and moderate caries.

Recently, Dayi et al. [39] provided an architecture for the Dental Caries Detection Network (DCDNet) to segment dental caries. The main characteristic of DCDNet is the presence of a Multi-Predicted Output (MPO) structure at the end. This is what makes it different from other segmentation architectures. Zhang et al. [40] combined the adult dataset with the children's dataset in order to show that, despite significantly increasing the number of children's datasets, the adult dataset did not enhance the experimental effects of the children's dental dataset.

The literature review reveals that previous studies have explored various methods for detecting and classifying dental caries. In addition to the research mentioned above, there are still some research gaps that need to be addressed in the field of dental cavity detection. Although some previous studies have focused on classifying teeth as decayed or normal, there is a need for a more specific and detailed identification of the different stages of dental caries, such as initial, moderate, or extensive caries. This level of classification can provide valuable information to make more targeted and effective decisions. One popular deep learning approach for image segmentation, used in [8,14,36,36,38] is the U-Net architecture. Several variants of U-Net have been proposed to improve its performance in dental caries segmentation, basically using either [21] or [22] as a base model. U-Net utilizes an encoder-decoder structure with skip connections, which allows for the combination of high-resolution features with the up-sampled output, resulting in improved segmentation performance.

Furthermore, in addition to assessing the detection performance of these models, several studies have also compared their diagnostic performance with that of clinicians, such as [8]. The results have shown that deep learning models can significantly improve clinicians' diagnostic performance in detecting dental caries and lesions on dental X-ray images. These findings highlight the potential of deep learning models to serve as valuable tools for clinicians with the diagnosis and treatment planning of dental caries [28]. Overall, a significant body of research has been conducted on the application of deep learning models in dental caries detection and diagnosis and has shown promising results [8].

However, one of the primary difficulties in segmenting dental caries, as mentioned in [8,11,36], is the unequal distribution of exposure to X-rays and variations in tooth density, thickness, or reflections of various structures and organs, particularly in panoramic images. These factors introduce irregularities into radiographic images, posing challenges for conventional segmentation techniques to precisely detect and outline carious lesions. In conclusion, the use of DL methods in dental cavity detection has shown promise in improving accuracy and reducing the workload of dentists. Various studies have explored different DL architectures such as NN and CNN to detect and classify dental caries in X-ray

images. These methods have demonstrated good detection performance, with accuracy scores ranging from 97% to 93.61%.

## 2. Methodology

CNN-based algorithms have allowed significant progress in the field of dental image segmentation and detection. U-Net is one of the DL networks that has performed well in medical image segmentation. In the following, we describe these networks in detail.

### 2.1. Models Employed

In the following, we summarize the most prominent models employed in teeth cavity segmentation

#### 2.1.1. U-Net

U-Net is a popular deep learning network used for medical image segmentation, as mentioned in [21]. U-Net is recognized for its encoder–decoder architecture, which is crucial for accurate segmentation. The U-Net structure consists of two key elements: the contraction path and the expansion path, which resembles a ‘U’ shape. In the contraction path, convolution operations are applied, followed by specific maximum pooling operations. On the other hand, the expansion path involves transposed convolution operations. This U-Net architecture includes two  $3 \times 3$  convolutions, the activation of the Rectified Linear Unit (ReLU), and  $2 \times 2$  maximum pooling with a stride of two for down sampling. In the up sampling path, they use  $2 \times 2$  transposed convolution operations to reduce the feature channels. An important feature of the U-Net is the inclusion of convolution path skip connections, which allow the transfer of features from the contraction path to the expansion path. This helps recover spatial features lost during down sampling operations, as explained in [35]. In total, the U-Net network consists of 23 convolutional layers as in [21].

#### 2.1.2. U-Net ++

To tackle the demand for improved segmentation of medical images, U-Net was enhanced through the creation of an architecture that incorporates nested and dense skip connections. This updated version was coined U-Net++ [22]. However, sufficient information has not been explored at full scale, and there is a need for further improvement [23].

#### 2.1.3. U-Net 3+

Huang et al. [23] introduced a novel architecture called U-Net 3+, which is based on the U-shaped design. This architecture uses full-scale skip connections and deep supervision. U-Net3+ was developed to address the limitations of previous U-Net variants and improve the performance of segmentation tasks, particularly in medical imaging. It has found successful applications in various real-world scenarios, including medical imaging, satellite imagery analysis, and industrial automation. This network architecture has shown promising results in these fields, showcasing its versatility and effectiveness in different domains. The extensibility and symmetry of the U-Net framework allow for a variety of possible designs. One such design is U-Net3+, which incorporates advanced features and optimizations to improve segmentation performance. U-Net3+ introduces advanced features that optimize feature utilization and incorporate attention-gate techniques for improved segmentation performance. These features allow U-Net3+ to surpass its predecessors in terms of accuracy and efficiency, making it a powerful tool for medical imaging and other applications.

According to [23], the low-level detailed feature maps capture intricate spatial information, highlighting organ boundaries, while the high-level semantic feature maps provide positional information about the organ locations. To fully harness the advantages of these multi-scale features, U-Net 3+ integrates low-level details with high-level semantics from the full-scale feature maps. Importantly, it accomplishes this with fewer parameters,

leading to improved computational efficiency. U-Net 3+ achieves this by redesigning skip connections and incorporating full-scale deep supervision.

By incorporating multi-scale features, redesigning skip connections, and utilizing multi-scale depth supervision, U-Net3+ can produce more accurate location-aware and boundary-enhanced segmentation maps. The use of multi-scale features in U-Net3+ enables the network to capture information at different resolutions, enhancing its ability to detect objects and boundaries of interest. Additionally, U-Net3+ leverages attention-gate techniques to focus on local semantic features, allowing the network to prioritize important regions of the image while suppressing non-interesting regions.

## 2.2. U-Net3+ Model for Cavity Segmentation

Image segmentation is one of the major topics in image processing and computer vision techniques. Image segmentation divides an image into several segments with similar features. Medical imaging, object detection, and recognition tasks are the fundamental applications of image segmentation. Medical image segmentation is a basic requirement in medical applications for diagnosing and identifying diseases [35]. Here, we describe the adaptation of U-Net 3+ ([23]) for the detection of dental cavities. U-Net 3+ is a DL-based segmentation method validated on two organs: the liver and the spleen [23]. To the best of our knowledge, we are the first to apply it in the dental field.

In this study, the contraction path follows the typical CNN architecture. The contraction path consists of the repeated application of two  $3 \times 3$  convolutions (Conv2D), each followed by a Gaussian error linear unit (GeLU) activation function with stride 2 for downsampling. It doubles the number of feature channels at each downsampling step. GeLU is a high-performance neural network activation function that aims to combine the properties of dropout and ReLU.

Conversely, the transposed convolution operation is performed in the expansion path. In each step of the expansion path, there is an up-sampling of the feature map followed by a  $2 \times 2$  convolution of up-scaled layers that has half the number of feature channels. Additionally, it concatenates with the correspondingly cropped feature map from the contracting path decoder blocks and two  $3 \times 3$  convolutions, each followed by the ReLU activation function. In the final layer, the output is a  $1 \times 1$  convolution layer with one output, predicted ground truth, which maps each 64-component feature vector to the desired number of classes.

U-Net 3+ combines the full-scale features by redesigning skip connections and using full-scale deep supervision. There are five encoder blocks and four decoder blocks in the architecture of this project. The numbers of filters are 32, 64, 128, 256, and 512. The addition of Gaussian noise (GN) to the input variables is the most common type of noise used. GN is a regularization layer for NN that is only active during training time and helps to mitigate over-fitting. It is also an important part of the feature-learning process. The GN function was applied to the U-Net 3+ model, then the dice loss function and Adam optimization algorithm were used to train the model. Dice loss is used in medical image segmentation to address the data imbalance problem. The flowchart of the entire project is illustrated and summarized in Figure 1.

## 2.3. Dataset Preparation Procedure

This article uses DNS Panoramic Images obtained from Ivisionlab [41]. The dataset comprises 1500 panoramic X-ray images with a binary mask that segments the tooth from other surfaces in the mouth. Since the available ground truth is unsuitable for the purpose of our evaluation, a new binary ground truth of cavities is created. Detailed steps for preparing the datasets for model evaluation are listed below.

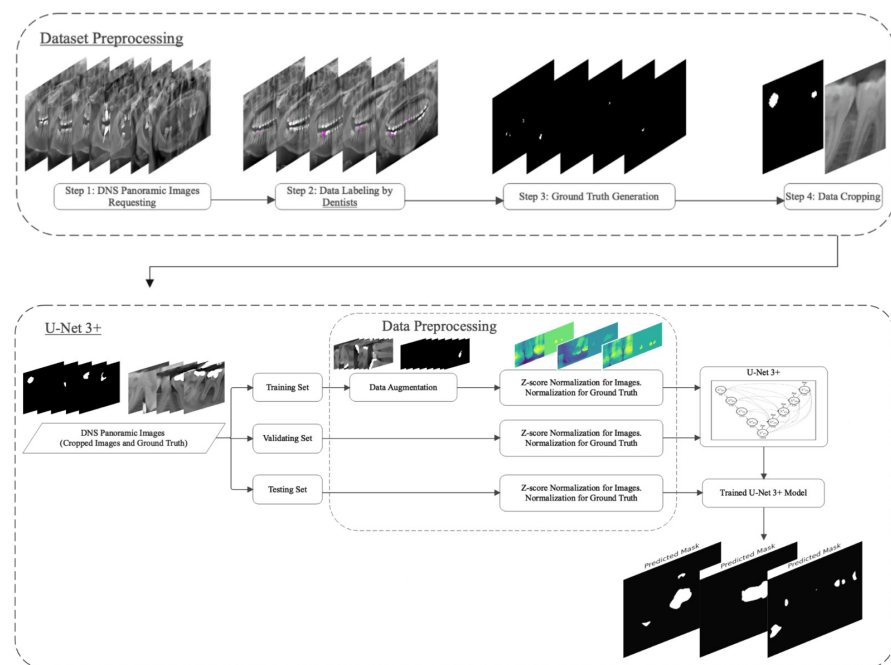


**Figure 1.** A brief overview of the steps followed to prepare and analyze the expanded Ivisionlab DNS panoramic dataset using U-Net3+ in order to detect tooth cavities.

### 2.3.1. Dataset Pre-Processing

The model reads the dataset and resizes the height and width of all images in the dataset to  $256 \times 256$  pixels. The images convert to grayscale, which will help to simplify the algorithm and reduce the computational requirements. A grayscale image is an image in which the only colors are shades of gray. Then, the model visualizes and combines the image with its ground truth for the training and testing process.

### 2.3.2. Dataset Normalization

The normalization in DL is one of the image preprocessing techniques that translates the image data's pixel values to a predefined range, usually  $(0-1)$  or  $(-1-1)$ , without changing its original nature. Another technique of normalization is called Z-score normalization. The Z-score is a strategy of normalizing every value in a dataset based on the mean and standard deviation such that the mean of all of the values is 0 and the standard deviation is 1. The Z-score normalization of the model is calculated by Equation (1):

$$Z = \frac{x - \mu}{\sigma}, \quad (1)$$

where  $x$  indicates the pixel value,  $\mu$  is the mean value of the feature, and  $\sigma$  is the standard deviation of the feature.

The benefit of the Z-score is that the clear outlier in the dataset is transformed in such a way that it is no longer a massive outlier. In addition, normalizing data using Z-scores is useful when dealing with data that have different scales and units, allowing us to compare their relative importance.

### 2.3.3. Data Annotation and Labelling

Since the available ground truth associated with this dataset is a binary mask that is used to segment teeth from other tissues, the ground truth associated with this dataset is unsuitable for the cavity study. Thus, a new binary ground truth of cavities had to be annotated.

At first, two dentists (thanks to Noura A. Alrogaibah and Ghadeer K. Aljarbou from the Primary Health Care Government Center in Qassim for labeling and reviewing the

ground truth of the dataset) marked the cavities in the images. All dentists were employees at the Ministry of Health in Saudi Arabia and had clinical experience of 5–8 years. As a result of marking images, only 510 of 1500 panoramic X-ray images have cavities. After marking the cavities in the dataset by dentists, the ground truth of the labeled dataset is generated using the ImageJ tool (<https://imagej.nih.gov/ij/> (accessed on 20 August 2023)) [42]. The number of images from the cropped dataset is 673 with dimensions of  $512 \times 512$  pixels. The annotation of the image showed that only 510 of the panoramic X-ray images of 1500 had cavities. Figure 2 presents some samples of the dataset after annotation of the cavities in the panoramic X-rays.

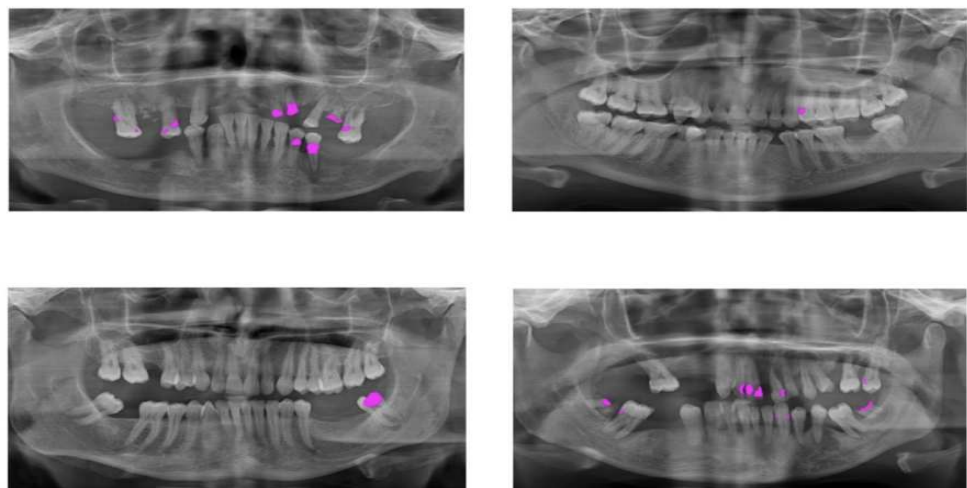


**Figure 2.** Sample panoramic X-ray images from Ivisionlab [41] after being annotated by two dentists. The cavity's location on the panoramic X-ray image is shown by the pink color.

In the second step, the ground truth of the labeled dataset was generated using the ImageJ tool. Figure 3 displays some sample ground truth images generated from the panoramic X-ray images with cavities.

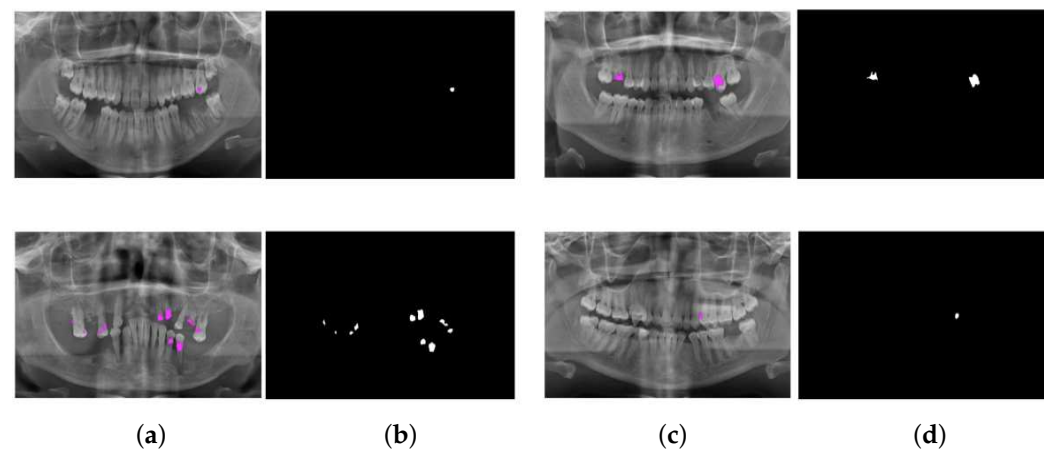


**Figure 3.** Sample panoramic X-ray images from Ivisionlab [41] associated with their ground truth. (a,c) Annotated images; pink indicates the location of the cavity on the panoramic X-ray image. (b,d) The ground truth that will be used as the ground truth for the model train. The white region indicates the segmented cavity.

The new ground truth had a large space of black color as a background and a small spot of white color corresponding to the cavity. This imbalance problem affected the performance in the cavity detection task since a large area of each image was the background. To improve the results, the images were cropped to reduce the unnecessary background and balance

the classes in the ground truth. Figure 4 presents some samples of the images and ground truth after the cropping process. The number of images in the cropped dataset was 673 with dimensions of  $512 \times 512$  pixels.

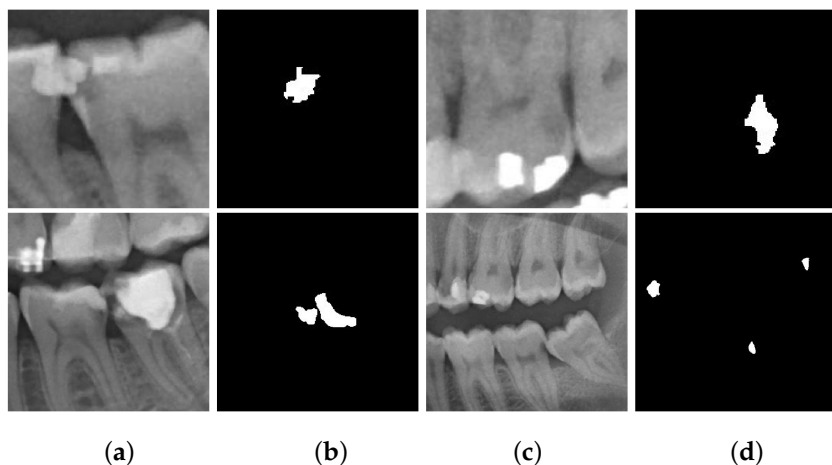


**Figure 4.** The samples of cropped images: (a,c) original cropped image and (b,d) ground truth.

#### 2.3.4. Data Augmentation

The lack of datasets is a major limitation in medical fields. Therefore, the data augmentation techniques must be applied to increase the number of images for better training of the model. Data augmentation is a method that creates a new set of images using existing ones to overcome the over-fitting. In this work, the techniques of data augmentation that were applied to the dataset are Horizontal flipping, Vertical flipping, Mirroring, and Rotation. Figure 5 shows an example of one image from the dataset and the images generated from the data augmentation process.

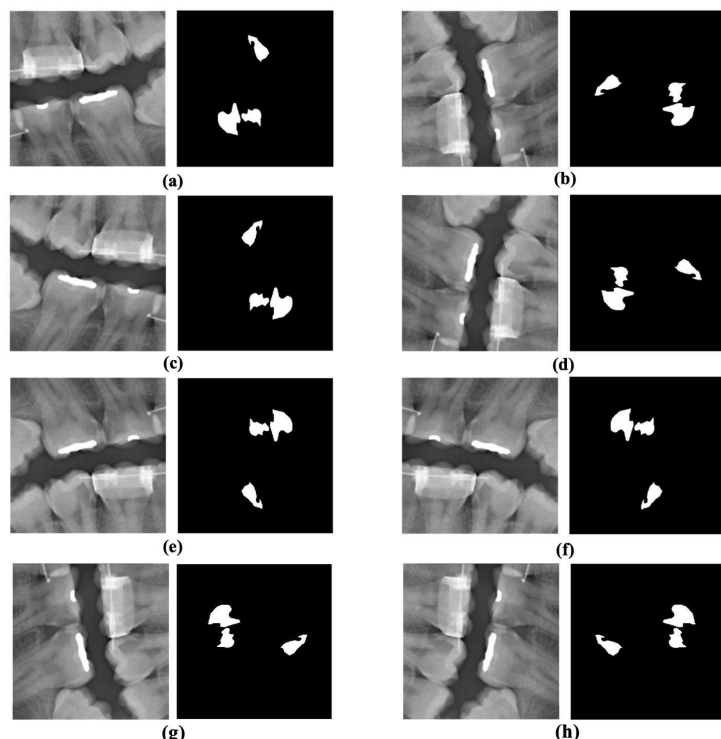


**Figure 5.** The samples of the augmented image: (a) Original. (b) Rotated 0 degrees. (c) Flipped horizontally. (d) Flipped vertically and rotated 90 degrees. (e) Flipped horizontally and vertically. (f) Flipped vertically. (g) Rotated 90 degrees. (h) Flipped vertically and rotated 90 degrees.

#### 2.4. Experimental Setup and Hyper-Parameters

This experiment was conducted in Python, in particular, Python3 [43]. To construct the network models, Keras [44] was used with Tensorflow [45] as the backend. In addition, the proposed method was trained and validated using the expandable Ivisionlab dataset as shown in Table 1.

**Table 1.** The details of the hyperparameters used in the evaluation of the models.

Hyperparameters	Value
Learning rate	0.0001
Optimizer	Adam
Activation function	gelu
Regularizers	No
Early Stopping	No
Batch size	4
Dropout	0.4
Dense activation function	ReLU

### 3. Results and Analysis

Throughout this section, we will provide a comprehensive analysis of the obtained results, highlighting the performance metrics and discussing notable findings and observations.

#### 3.1. Evaluation Matrices Used in Models Comparison

In this work, we evaluate the model performance by using the Mean Squared Error (MSE) as a loss function, the Intersection over Union (IoU), the Dice coefficient, and accuracy evaluation matrices. The details of these evaluation matrices are displayed in Table 2.

**Table 2.** A brief overview of the performance metrics used in the model evaluation.

Metrics	Formula	Definition
Mean Squared Error (MSE)	$\frac{1}{N} \sum_i^N (Y_i - \hat{Y}_i)^2$ (1)	Function that determines how much the values that were predicted and those that were observed differ.
Intersection over Union (IoU)	$\frac{TP}{TP+FN+FP}$ (2)	It is used to identify which members are similar and which are distinct; this index calculates the degree of similarity between two groups of members.
Dice	$\frac{2 \times \text{Area of overlap}}{\text{Total area}}$	It is used to assess how closely a predicted segmentation mask and the ground truth segmentation mask resemble each other.
Accuracy	$\frac{TP+TN}{TP+TN+FP+FN}$ (2)	It is determined by the number of correctly predicted data points.

<sup>1</sup>  $N$  refers to the number of data points,  $Y_i$  to the observed values and  $\hat{Y}_i$  to the predicted values. <sup>2</sup> TP refers to true positives, TN to true negatives, FP to false positives, and FN to false negatives.

#### 3.2. Quantitative Validation

The model was trained on the dataset before cropping the images with a test size of 0.1. The result showed that the IoU was good during the training process but very low during the testing phase. The ground truth of the uncropped panoramic images had a large space of black color (background) and a small spot of white color (cavity). Due to

this, the accuracy was low in the cavity detection model because the accuracy dealt with the background as “True Positive”; therefore, the accuracy for this model performance was unreasonably high. To address this problem, the dataset was cropped to obtain an image with only the tooth that has a cavity. After training the model with sizes of the test set of 0.1 and 0.2 from the dataset, the result showed that the IoU was good during the training process but low during the testing phase.

The Dice coefficient was very good during the training process but very low during the testing. Accuracy was good during both the training and the testing process. The model was trained in numerous splitting conditions to check the performance and obtain the best results. Table 3 illustrates the split size of the dataset during the experiments.

**Table 3.** The size of the dataset during the evaluation of the models.

Dataset	Train	Validate	Test	Total
Original without cropping and augmentation	459	-	51	510
Dataset after cropping	605	-	68	673
Dataset with 80–20% split and augmentation	4296	-	136	4432
Dataset with 90–10% split and augmentation	4840	-	68	4908
Dataset with 80–10–10% split and augmentation	4296	68	68	4432
Dataset with 60–40% validation size: 0.1 and augmentation	2887	321	272	3480

These extensive experiments showed that the data-splitting process did not affect or enhance the result of the model performance. In this study, the performance is dependent on the type of dataset and the target lesion for detection. The dental panoramic image is more difficult to analyze than another type of dental X-ray. The panoramic radiograph contains shadows that are reflections of various structures and organs, such as the lips. It also contains dark spots, such as spots in the roots. Those shadows and spots confused the training process and affected the model’s performance. Additionally, the quality of panoramic X-rays is essential for accurately detecting cavities or any lesions. Some panoramic X-rays are poor quality, making it difficult to detect abnormal lesions. Table 4 presents the performance results of U-Net, U-Net++, and U-Net 3+ in the training, validation, and test sets with an 80–10–10% split of the dataset (Train: 4296, Val: 68, Test: 68). Figures 6–8 illustrate the results in the training and validation of the dataset with an 80–10–10% split and using different U-Net family models.

**Table 4.** The performance results of U-Net, U-Net++, and U-Net 3+ in the training and validation sets with an 80%/10%/10% split of the dataset for training, validation, and testing, respectively (Train: n = 4296, Val: n = 68, Test: n = 68).

Model	Task	loss	IoU	Dice	Accuracy
U-Net	Training	0.07	0.77	0.92	0.98
	Validating	0.39	0.67	0.60	0.95
	Testing	0.41	0.67	0.58	0.95
U-NET++	Training	0.10	0.77	0.89	0.98
	Validating	0.50	0.62	0.49	0.95
	Testing	0.47	0.65	0.53	0.95
U-Net 3+	Training	0.09	0.77	0.90	0.98
	Validating	0.48	0.62	0.51	0.95
	Testing	0.44	0.67	0.60	0.95

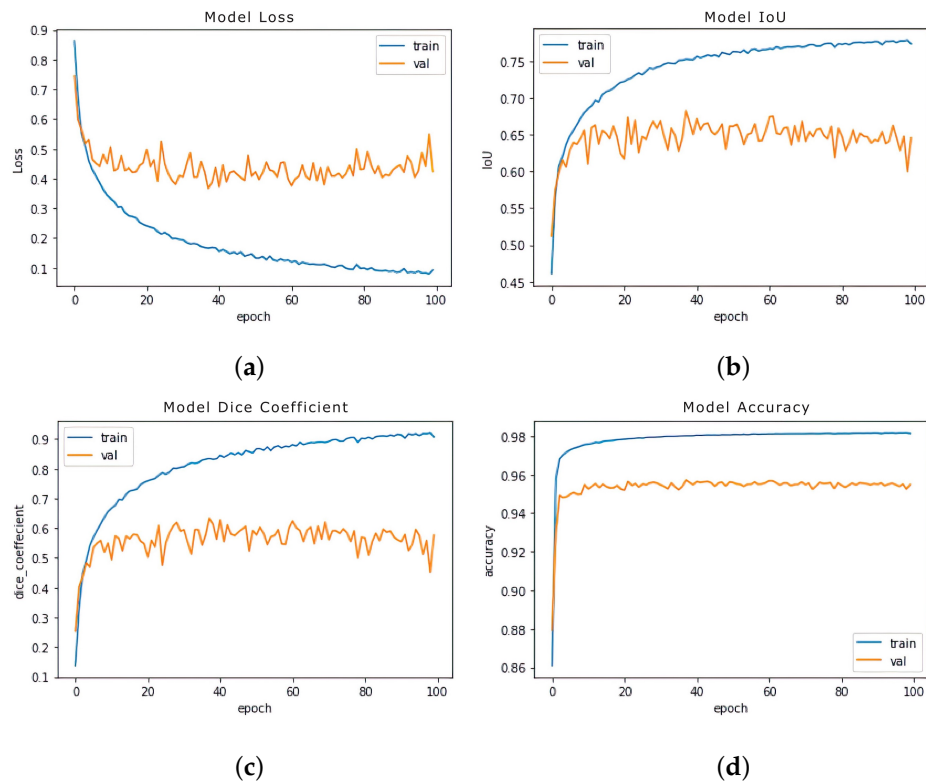


**Figure 6.** Performance analysis of U-Net for the training and validation sets. The dataset was split to 80%/10%/10% for training and validation, respectively: (a) Loss function. (b) Intersection over the Union. (c) Dice coefficient. (d) Accuracy.

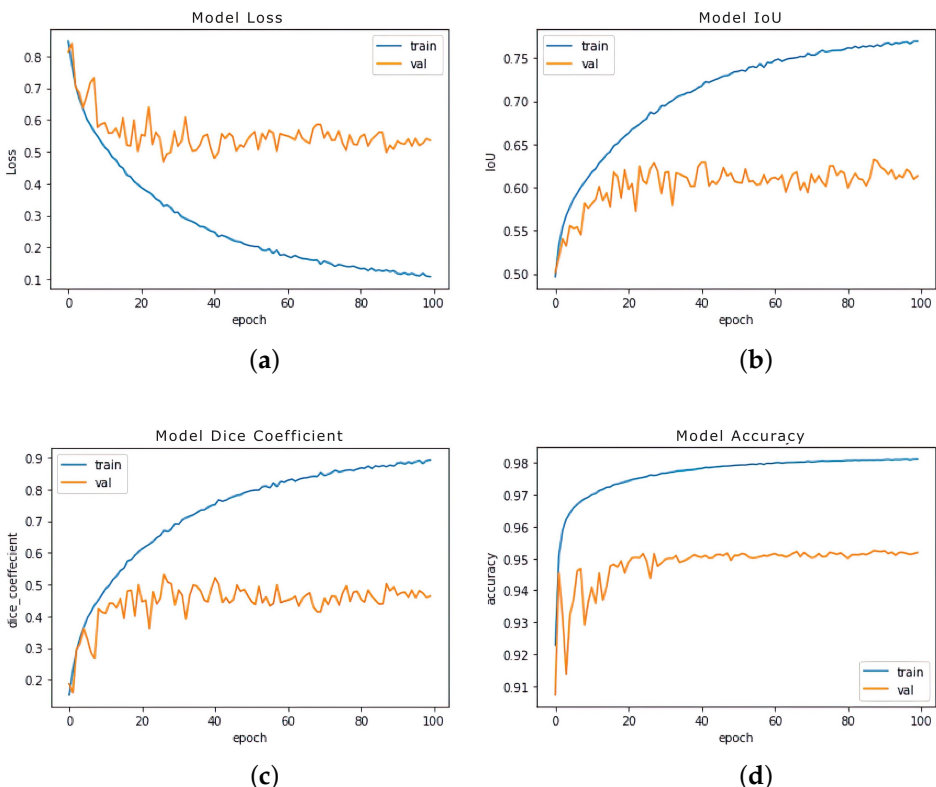


**Figure 7.** Performance analysis of U-Net++ for the training and validation sets. The dataset was split into 80%/10%/10% for training and validation, respectively: (a) Loss function. (b) Intersection over the Union. (c) Dice coefficient. (d) Accuracy.

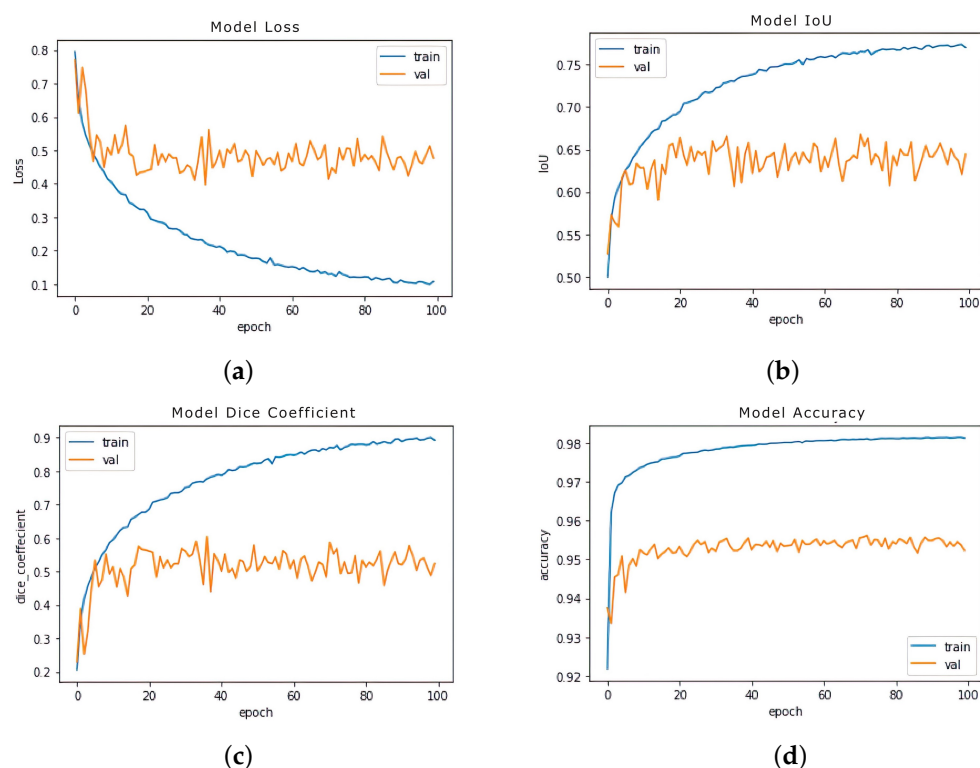


**Figure 8.** The performance results of U-Net 3+ in the training and validation sets. The dataset split to 80/10/10 for training and validation, respectively: (a) Loss function. (b) Intersection over the Union. (c) Dice coefficient. (d) Accuracy.

Accordingly, Table 5 presents the best results of cavity detection by using U-Net 3+ in the training and validation sets of the dataset with a 60–40% split and validating sizes of 0.1. Based on the training and validation of the dataset, Figure 9 illustrates the best performance results.

These extensive experiments showed that the data-splitting process did not affect or enhance the result of the model performance. In this study, the performance is dependent on the type of dataset and the target lesion for detection.

**Table 5.** The best performance results of U-Net 3+ with a 60–40% validation size: 0.1 and augmentation for the training and validation and a 80–10–10% split for testing.

<b>Dataset</b>	<b>IoU</b>	<b>Dice</b>	<b>Accuracy</b>
Training	0.77	0.89	0.98
Validating	0.77	0.90	0.98
Testing	0.67	0.60	0.95

### 3.3. Qualitative Validation

Additionally, as displayed in Figure 10, we display a sample of the segmentation results using different nested U-Net models. It is notable that U-Net3+ [23] outperformed compared with other methods discussed in the literature [21,22]. This is because U-Net3+ improves its detection capabilities of objects and borders of interest by allowing the network to gather data at various resolutions.

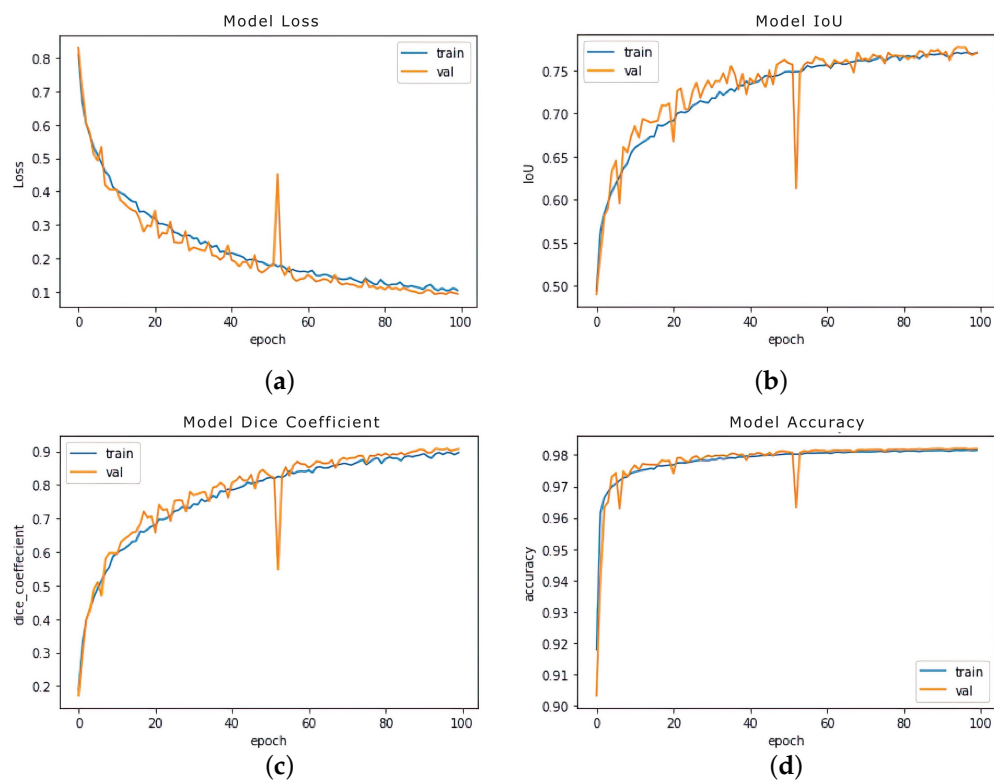


**Figure 9.** The best performance results of U-Net 3+ in the training and validation sets. The dataset was split to 60%/40% (training/validation) with validation size = 0.1: (a) Loss function. (b) Intersection over the Union. (c) Dice coefficient. (d) Accuracy.

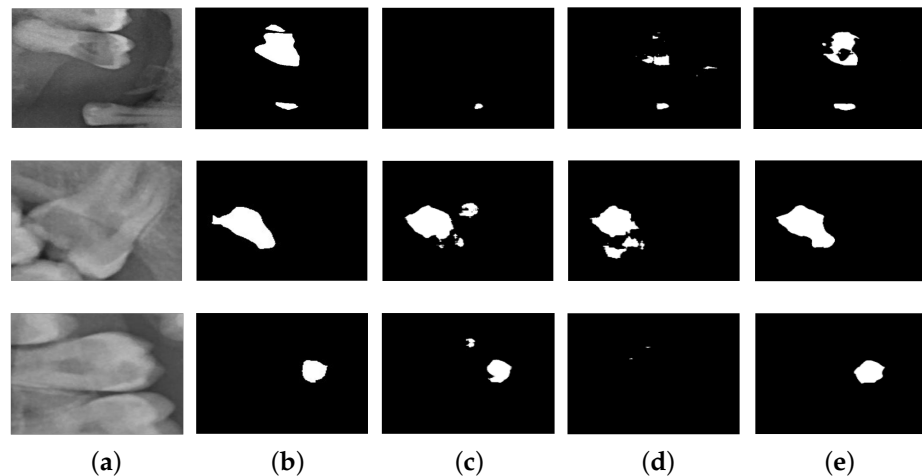


**Figure 10.** Samples of panoramic X-ray images from the IvisionLab dataset were used for the qualitative validation and comparison of the various U-Net shape models: (a) Original image. (b) Ground truth. (c) U-Net. (d) U-Net++. (e) U-Net3+.

As discussed earlier in Section 1, X-rays have many problems in the quality of acquisition, which caused difficulties in data training, especially the dental panoramic image. The panoramic radiograph contains shadows that are reflections of various structures and organs, such as the lips. It also contains dark spots such as spots in the roots. Those shadows and spots confused the training process and affected the model's performance. Additionally, the quality of panoramic X-rays is essential for accurately detecting cavities or any lesions. Some panoramic X-rays are poor quality, making it difficult to detect abnormal lesions. Figure 11 presents some examples of shadows and dark areas on panoramic X-rays.

Usually, the dentist is familiar with these areas and can determine if this is a lesion or a fake spot. In contrast, the deep learning models may fail to identify these issues.

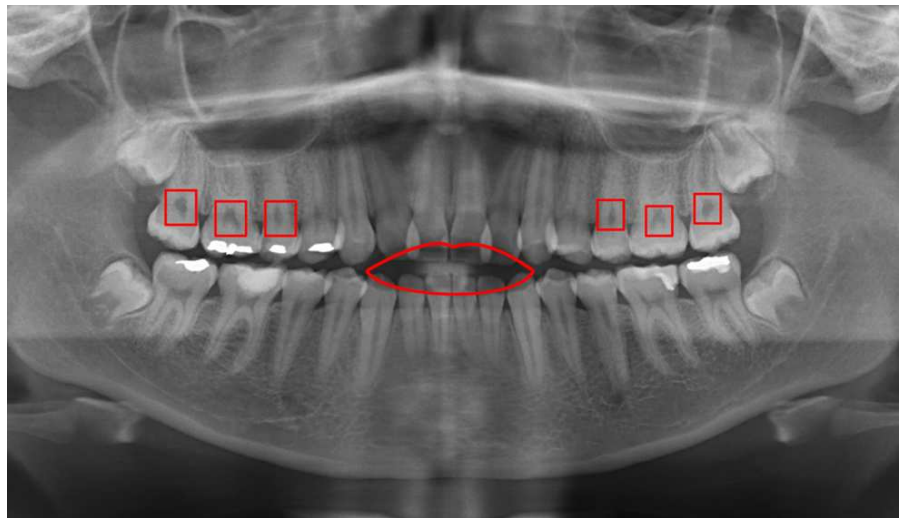


**Figure 11.** An example image from the Ivisionlab dataset that illustrates the drawbacks of panoramic images in which the red color indicates the shadows of the tongue and gingival pocket.

#### 4. Conclusions

Dental cavities are one of the most prevalent and chronic diseases worldwide. The early detection of dental caries lesions can prevent tooth damage and save expensive healthcare costs. U-Net is one of the CNN architectures that has become most popular and widely applied in medical image segmentation. However, there are a few studies on applying the U-Net or CNN-based U-Net architecture in dental caries detection.

Although the dental panoramic image is clinically helpful for the diagnosis of dental diseases such as caries, it is difficult to interpret because it contains such a large area of anatomy with numerous superpositions of the hard and soft tissue structures of the region. A limited number of datasets with their ground truth labeling are available for deep learning training and validation. Thus, in this work, we extended the Ivisionlab DNS Panoramic Dataset by annotation of the cavity in X-ray images and used them as ground truth to train the U-Net modules.

Moreover, for cavity detection, this work utilized the U-Net 3+ model, which is a modified version of U-Net and U-Net++ by combining the multiscale features by redesigning the skip connections and using full-scale deep supervision for more accurate medical image segmentation. The results of cavity segmentation was compared with those of different U-Net architectures and different data-splitting ratios. According to these extensive experiments, data splitting did not affect or enhance the performance of the model. U-Net 3+ performed better compared to U-Net and U-Net ++, with 95% segmentation accuracy. The reason for this is that U-Net 3+ utilizes full-scale skip connections, and deep supervisions were used; the use of dense and nested skip connections in the contract prevented U-Net and U-Net++ from detecting enough information from the full scale (i.e., cavity).

#### 5. Future Work

In order to improve uniformity and generalizability, future research must incorporate the following elements: our work's evaluation studies only used one kind of modality, so it would be interesting to include a multi-modality imaging of dental radiography while assessing the models. Furthermore, additional recent CNN models, such as Ref-U-Net 3+ [46], CMFCUNet [47] and LMNS-Net [48], could be used to improve performance. Hypermodels (two or more models combined in a single detection) can be used to improve the accuracy of cavity segmentation. More research in the future should be conducted to test this assumption.

**Author Contributions:** Conceptualization, S.S.A.; Methodology, S.S.A. and A.A.A.; Validation, S.S.A. and A.A.A.; Formal analysis, S.S.A. and H.F.A.; Investigation, S.S.A.; Resources, A.A.A.; Writing—original draft, S.S.A.; Writing—review & editing, H.F.A. and R.U.K.; Visualization, A.A.A.; Supervision, S.S.A.; Project administration, S.S.A. All authors have read and agreed to the published version of the manuscript

**Funding:** This research was funded by the Deanship of Scientific Research at Qassim University.

**Institutional Review Board Statement:** Not applicable.

**Informed Consent Statement:** Not applicable.

**Data Availability Statement:** The data presented in this study are available on request from the corresponding author due to privacy and ethical restrictions.

**Acknowledgments:** Researchers would like to thank the Deanship of Scientific Research, Qassim University for funding publication of this project.

**Conflicts of Interest:** The authors declare no conflict of interests.

## References

1. Selwitz, R.H.; Ismail, A.I.; Pitts, N.B. Dental caries. *Lancet* **2007**, *369*, 51–59. [[CrossRef](#)] [[PubMed](#)]
2. Mardiah, A. Improving Awareness and Clean and Healthy Living Behavior among Students in Preventing Dental Caries. *Path Sci.* **2023**, *9*, 7. [[CrossRef](#)]
3. Machiulskiene, V.; Campus, G.; Carvalho, J.C.; Dige, I.; Ekstrand, K.R.; Jablonski-Momeni, A.; Maltz, M.; Manton, D.J.; Martignon, S.; Martinez-Mier, E.A.; et al. Terminology of dental caries and dental caries management: Consensus report of a workshop organized by ORCA and Cariology Research Group of IADR. *Caries Res.* **2020**, *54*, 7–14. [[CrossRef](#)] [[PubMed](#)]
4. Pitts, N.B.; Zero, D.T.; Marsh, P.D.; Ekstrand, K.; Weintraub, J.A.; Ramos-Gomez, F.; Tagami, J.; Twetman, S.; Tsakos, G.; Ismail, A. Dental caries. *Nat. Rev. Dis. Prim.* **2017**, *3*, 1–16. [[CrossRef](#)] [[PubMed](#)]
5. Huang, Y.P.; Lee, S.Y. An Effective and Reliable Methodology for Deep Machine Learning Application in Caries Detection. *medRxiv* **2021**, 21256502.
6. Casalegno, F.; Newton, T.; Daher, R.; Abdelaziz, M.; Lodi-Rizzini, A.; Schürmann, F.; Krejci, I.; Markram, H. Caries Detection With Near-Infrared Transillumination Using Deep Learning. *J. Dent. Res.* **2019**, *98*, 1227–1233. [[CrossRef](#)] [[PubMed](#)]
7. Gordan, V.V.; Riley, J.L., III; Carvalho, R.M.; Snyder, J.; Sanderson, J., Jr.; Anderson, M.; Gilbert, G.; Group, D.C. Methods used by Dental Practice-based Research Network (DPBRN) dentists to diagnose dental caries. *Oper. Dent.* **2011**, *36*, 2–11. [[CrossRef](#)]
8. Lee, S.; Oh, S.I.; Jo, J.; Kang, S.; Shin, Y.; Park, J.W. Deep Learning for Early Dental Caries Detection in Bitewing Radiographs. *Sci. Rep.* **2021**, *11*, 16807 [[CrossRef](#)]
9. Sharma, M.; Kumar, N. Improved hepatocellular carcinoma fatality prognosis using ensemble learning approach. *J. Ambient. Intell. Humaniz. Comput.* **2022**, *13*, 5763–5777. [[CrossRef](#)]
10. Kumaraswamy, E.; Kumar, S.; Sharma, M. An Invasive Ductal Carcinomas Breast Cancer Grade Classification Using an Ensemble of Convolutional Neural Networks. *Diagnostics* **2023**, *13*, 1977. [[CrossRef](#)]
11. Huang, C.; Wang, J.; Wang, S.; Zhang, Y. A review of deep learning in dentistry. *Neurocomputing* **2023**, *2023*, 126629. [[CrossRef](#)]
12. Ding, H.; Wu, J.; Zhao, W.; Matinlinna, J.P.; Burrow, M.F.; Tsoi, J.K. Artificial intelligence in dentistry—A review. *Front. Dent. Med.* **2023**, *4*, 1085251. [[CrossRef](#)]
13. Duong, D.L.; Kabir, M.H.; Kuo, R.F. Automated Caries Detection With Smartphone Color Photography Using Machine Learning. *Health Inform. J.* **2021**, *27*, 14604582211007530. [[CrossRef](#)] [[PubMed](#)]
14. Zheng, Z.; Yan, H.; Setzer, F.C.; Shi, K.J.; Mupparapu, M.; Li, J. Anatomically Constrained Deep Learning For Automating Dental cbct Segmentation And Lesion Detection. *IEEE Trans. Autom. Sci. Eng.* **2020**, *18*, 603–614. [[CrossRef](#)]
15. Prados-Privado, M.; García Villalón, J.; Martínez-Martínez, C.H.; Ivorra, C.; Prados-Frutos, J.C. Dental Caries Diagnosis and Detection Using Neural Networks: A Systematic Review. *J. Clin. Med.* **2020**, *9*, 3579. [[CrossRef](#)] [[PubMed](#)]
16. Kermany, D.S.; Goldbaum, M.; Cai, W.; Valentim, C.C.; Liang, H.; Baxter, S.L.; McKeown, A.; Yang, G.; Wu, X.; Yan, F.; et al. Identifying medical diagnoses and treatable diseases by image-based deep learning. *Cell* **2018**, *172*, 1122–1131. [[CrossRef](#)] [[PubMed](#)]
17. Alom, M.Z.; Yakopcic, C.; Hasan, M.; Taha, T.M.; Asari, V.K. Recurrent residual U-Net for medical image segmentation. *J. Med. Imaging* **2019**, *6*, 014006. [[CrossRef](#)]
18. Gu, Z.; Cheng, J.; Fu, H.; Zhou, K.; Hao, H.; Zhao, Y.; Zhang, T.; Gao, S.; Liu, J. Ce-net: Context encoder network for 2d medical image segmentation. *IEEE Trans. Med. Imaging* **2019**, *38*, 2281–2292. [[CrossRef](#)]
19. Viniavsky, O.; Dobko, M.; Dobosevych, O. Weakly-supervised segmentation for disease localization in chest X-ray images. In Proceedings of the International Conference on Artificial Intelligence in Medicine, Minneapolis, MN, USA, 25–28 August 2020; pp. 249–259.
20. Wang, R.; Lei, T.; Cui, R.; Zhang, B.; Meng, H.; Nandi, A.K. Medical image segmentation using deep learning: A survey. *IET Image Process.* **2022**, *16*, 1243–1267. [[CrossRef](#)]

21. Ronneberger, O.; Fischer, P.; Brox, T. Dental X-ray image segmentation using a U-shaped Deep Convolutional network. In Proceedings of the International Symposium on Biomedical Imaging, New York, NY, USA, 16–19 April 2015; Volume 1, p. 3.
22. Zhou, Z.; Siddiquee, M.M.R.; Tajbakhsh, N.; Liang, J. Unet++: A nested u-net architecture for medical image segmentation. In *Deep Learning in Medical Image Analysis and Multimodal Learning for Clinical Decision Support*; Springer: Granada, Spain 2018; pp. 3–11.
23. Huang, H.; Lin, L.; Tong, R.; Hu, H.; Zhang, Q.; Iwamoto, Y.; Han, X.; Chen, Y.W.; Wu, J. Unet 3+: A full-scale connected unet for medical image segmentation. In Proceedings of the IEEE International Conference on Acoustics, Speech and Signal Processing (ICASSP), Barcelona, Spain, 4–8 May 2020; pp. 1055–1059.
24. Albahbah, A.A.; El-Bakry, H.M.; Abd-Elgahany, S. Detection of caries in panoramic dental X-ray images using back-propagation neural network. *Int. J. Electron. Commun. Eng.* **2016**, *7*, 250.
25. Ali, R.B.; Ejbali, R.; Zaied, M. Detection and classification of dental caries in X-ray images using deep neural networks. In Proceedings of the International Conference on Software Engineering Advances (ICSEA), Rome, Italy, 21–25 August 2016.
26. Schwendicke, F.; Elhennawy, K.; Paris, S.; Friebertshäuser, P.; Krois, J. Deep Learning For Caries Lesion Detection In Near-Infrared Light Transillumination Images: A Pilot Study. *J. Dent.* **2020**, *92*, 103260. [CrossRef] [PubMed]
27. Haghifar, A.; Majdabadi, M.M.; Ko, S.B. Paxnet: Dental Caries Detection in Panoramic X-ray Using Ensemble Transfer Learning and Capsule Classifier. *arXiv Prepr.* **2020**, arXiv:2012.13666.
28. Lian, L.; Zhu, T.; Zhu, F.; Zhu, H. Deep Learning for Caries Detection and Classification. *Diagnostics* **2021**, *11*, 1672. [CrossRef] [PubMed]
29. Moran, M.; Faria, M.; Giraldi, G.; Bastos, L.; Oliveira, L.; Conci, A. Classification of Approximal Caries in Bitewing Radiographs Using Convolutional Neural Networks. *Sensors* **2021**, *21*, 5192. [CrossRef] [PubMed]
30. Kühnisch, J.; Meyer, O.; Hesenius, M.; Hickel, R.; Gruhn, V. Caries detection on intraoral images using artificial intelligence. *J. Dent. Res.* **2022**, *101*, 158–165. [CrossRef] [PubMed]
31. Lee, J.H.; Kim, D.H.; Jeong, S.N.; Choi, S.H. Detection And Diagnosis of Dental Caries Using A Deep Learning-Based Convolutional Neural Network Algorithm. *J. Dent.* **2018**, *77*, 106–111. [CrossRef] [PubMed]
32. Zhang, X.; Liang, Y.; Li, W.; Liu, C.; Gu, D.; Sun, W.; Miao, L. Development and Evaluation Of Deep Learning For Screening Dental Caries From Oral Photographs. *Oral Dis.* **2020**, *28*, 173–181. [CrossRef]
33. Bouchahma, M.; Hammouda, S.B.; Kouki, S.; Alshemaili, M.; Samara, K. An automatic dental decay treatment prediction using a deep convolutional neural network on X-ray images. In Proceedings of the IEEE/ACS 16th International Conference on Computer Systems and Applications (AICCSA), Abu Dhabi, United Arab Emirates, 3–7 November 2019; pp. 1–4.
34. Lee, S.; Woo, S.; Yu, J.; Seo, J.; Lee, J.; Lee, C. Automated CNN-Based Tooth Segmentation In Cone-Beam CT For Dental Implant Planning. *IEEE Access* **2020**, *8*, 50507–50518. [CrossRef]
35. Sivagami, S.; Chitra, P.; Kailash, G.S.R.; Muralidharan, S. Unet architecture based dental panoramic image segmentation. In Proceedings of the International Conference on Wireless Communications Signal Processing and Networking (WiSPNET), Chennai, India, 4–6 August 2020; pp. 187–191.
36. Cantu, A.G.; Gehrung, S.; Krois, J.; Chaurasia, A.; Rossi, J.G.; Gaudin, R.; Elhennawy, K.; Schwendicke, F. Detecting Caries Lesions of Different Radiographic Extension on Bitewings Using Deep Learning. *J. Dent.* **2020**, *100*, 103425. [CrossRef]
37. Khan, H.A.; Haider, M.A.; Ansari, H.A.; Ishaq, H.; Kiyani, A.; Sohail, K.; Muhammad, M.; Khurram, S.A. Automated feature detection in dental periapical radiographs by using deep learning. *Oral Surgery Oral Med. Oral Pathol. Oral Radiol.* **2021**, *131*, 711–720. [CrossRef]
38. Zhu, H.; Cao, Z.; Lian, L.; Ye, G.; Gao, H.; Wu, J. CariesNet: A deep learning approach for segmentation of multi-stage caries lesion from oral panoramic X-ray image. *Neural Comput. Appl.* **2022**, *35*, 16051–16059. [CrossRef] [PubMed]
39. Dayı, B.; Üzen, H.; Çiçek, İ.B.; Duman, Ş.B. A Novel Deep Learning-Based Approach for Segmentation of Different Type Caries Lesions on Panoramic Radiographs. *Diagnostics* **2023**, *13*, 202. [CrossRef] [PubMed]
40. Zhang, Y.; Ye, F.; Chen, L.; Xu, F.; Chen, X.; Wu, H.; Cao, M.; Li, Y.; Wang, Y.; Huang, X. Children’s dental panoramic radiographs dataset for caries segmentation and dental disease detection. *Sci. Data* **2023**, *10*, 380. [CrossRef] [PubMed]
41. Silva, B.; Pinheiro, L.; Oliveira, L.; Python, M. A study on tooth segmentation and numbering using end-to-end deep neural networks. In Proceedings of the Conference on Graphics, Patterns and Images (SIBGRAPI), Porto de Galinhas, Brazil, 7–10 November 2020; pp. 164–171.
42. Schindelin, J.; Arganda-Carreras, I.; Frise, E.; Kaynig, V.; Longair, M.; Pietzsch, T.; Preibisch, S.; Rueden, C.; Saalfeld, S.; Schmid, B.; et al. Fiji: An open-source platform for biological-image analysis. *Nat. Methods* **2012**, *9*, 676–682. [CrossRef] [PubMed]
43. Van Rossum, G.; Python Programming Language. In Proceedings of the USENIX Annual Technical Conference, Santa Clara, CA, USA, 17–22 June 2007; Volume 41, pp. 1–36.
44. Ketkar, N.; Ketkar, N. Introduction to keras. *Deep. Learn. Python Hands- Introd.* **2017**, 97–111.
45. Abadi, M.; Barham, P.; Chen, J.; Chen, Z.; Davis, A.; Dean, J.; Devin, M.; Ghemawat, S.; Irving, G.; Isard, M.; et al. Tensorflow: A system for large-scale machine learning. In Proceedings of the Osdi, Savannah, GA, USA, 2–4 November 2016; Volume 16, pp. 265–283.
46. Xu, Y.; Hou, S.; Wang, X.; Li, D.; Lu, L. A Medical Image Segmentation Method Based on Improved UNet 3+ Network. *Diagnostics* **2023**, *13*, 576. [CrossRef] [PubMed]

47. Qiu, C.; Song, Y.; Liu, Z.; Yin, J.; Han, K.; Liu, Y. CMFCUNet: Cascaded multi-scale feature calibration UNet for pancreas segmentation. *Multimed. Syst.* **2023**, *29*, 871–886. [[CrossRef](#)]
48. Paithane, P.; Kakarwal, S. LMNS-Net: Lightweight Multiscale Novel Semantic-Net deep learning approach used for automatic pancreas image segmentation in CT scan images. *Expert Syst. Appl.* **2023**, *234*, 121064. [[CrossRef](#)]

**Disclaimer/Publisher’s Note:** The statements, opinions and data contained in all publications are solely those of the individual author(s) and contributor(s) and not of MDPI and/or the editor(s). MDPI and/or the editor(s) disclaim responsibility for any injury to people or property resulting from any ideas, methods, instructions or products referred to in the content.